INTERNATIONAL JOURNAL FOR NUMERICAL METHODS IN FLUIDS, VOL. 9, 1395–1411 (1989)

CONVERGENCE PROPERTIES OF HIGH-REYNOLDS-NUMBER SEPARATED FLOW CALCULATIONS

S. G. RUBIN AND A. HIMANSU

Department of Aerospace Engineering & Engineering Mechanics, University of Cincinnati, Cincinnati, OH 45221, U.S.A.

SUMMARY

The convergence properties of an iterative solution technique for the Reduced Navier–Stokes equations are examined for two-dimensional steady subsonic flow over bump and trough geometries. Techniques for decreasing the sensitivity to the initial pressure approximation, for fine meshes in particular, are investigated. They are shown to improve the robustness of the relaxation process and to decrease the computational work required to obtain a converged solution. A semi-coarsening multigrid technique that has previously been found to be particularly advantageous for high-Reynolds-number (*Re*) flows with flow separation and with highly stretched surface-normal grids is applied herein to further accelerate convergence. Solutions are obtained for the laminar flow over a trough that is more severe than has been considered to date. Sufficient axial grid refinement in this case leads to a shock-like reattachment and, for sufficiently large *Re*, to a local 'divergence' of the numerical computations. This 'laminar flow breakdown' appears to be related to an instability associated with high-frequency fine-grid modes that are not resolvable with the present modelling. This behaviour may be indicative of dynamic stall or of incipient transition. The breakdown or instability is shown to be controllable by suitable introduction of transition turbulence models or by laminar flow control, i.e. small amounts of wall suction. This lends further support to the hypothesis that the instability is of a physical rather than numerical character and suggests that full three-dimensional analysis is required to properly capture the flow behaviour. Another inference drawn from this investigation is that there is a need for careful grid refinement studies in high-*Re* flow computations, since coarser grids may yield oscillation-free solutions that cannot be obtained on finer grids.

KEY WORDS Reduced Navier–Stokes computations Flow separation Laminar instability

1. INTRODUCTION

Numerical solutions to the full Navier–Stokes (NS) equations typically require considerable computational resources in order to accurately solve fluid flow problems that are of current interest. For this reason, in many studies sufficient grid refinement has not been possible. In recent years, it has been shown by Rubin and co-workers that for a large class of flow problems the full NS equations can be approximated, with negligible loss in accuracy, by the Reduced Navier–Stokes (RNS) system, for which only selected viscous terms have been omitted. The primary advantage of the RNS approximation is improved computational efficiency, i.e. fewer iterations and less storage; this enables very fine mesh calculations to be considered. By using an appropriate co-ordinate system, in which the omitted diffusion terms can be shown to be negligible, a variety of flows involving strong viscous–inviscid interaction, axial flow separation, shock interaction and upstream influence have been computed with the RNS model. The ellipticity of the equations is characterized by inviscid (acoustic) pressure interaction rather than by axial viscous diffusion. This is reflected in the formulation of an unconditionally stable line

0271–2091/89/111395–17$08.50

Received September 1988
Revised January 1989

relaxation solution procedure presented in several earlier studies; see e.g. Rubin[1] and Rubin and Reddy.[2] This iterative procedure uses marching sweeps, from inflow to outflow, to systematically decrease the error of the globally stored pressure field. The velocities are regenerated during each sweep. This algorithm has been applied to the computation of several incompressible, subsonic/transonic and supersonic steady flows with strong interaction and/or upstream influence by Rubin, Khosla and co-workers.

The convergence rates of the relaxation procedure slow down markedly with fine axial meshes and for large-*Re* flow; the solutions are typically very sensitive to grid stretching and distribution in the direction normal to the shear layer or surface boundary layer. Standard full-coarsening multigrid techniques for convergence acceleration have not been successful for viscous flows with highly stretched boundary layer meshes. An effective multigrid technique for such grids was developed in Reference 3 by the present authors and was used to obtain considerable enhancement of the convergence of the basic relaxation algorithm. The technique applies the multigrid philosophy only in the streamwise direction and is termed a semi-coarsening multigrid method.

As is the case with all iterative procedures for non-linear equations, the relaxation scheme is also sensitive to the assumed pressure field that is used to start the calculations. A poor initialization of the pressure will increase the computational effort required to obtain a converged solution and, for severe flow conditions and geometries, may even lead to divergence. In the present study, computationally economical strategies are sought whereby convergence can be further accelerated or the relaxation made significantly more robust by improvement of the initial pressure field approximation used to begin the iterative calculation process. The strategies include the introduction of temporal relaxation, preliminary inviscid flow computation and interpolation of coarse-grid calculations.

The accelerated RNS pressure relaxation scheme is used to investigate the flow over a smooth bump and a trough under more severe conditions than previously reported. For these cases, as discussed in Reference 3, divergence of the numerical iterations can be encountered with fine streamwise meshes. Theoretical analysis and the reporting of similar phenomena for a sine-wave bump geometry[4] lead to speculation that the 'instability' is of a physical nature. In the present study, this 'breakdown' is more thoroughly investigated on very fine meshes. The effects of a transition turbulence model and that of flow control with boundary layer suction applied in the neighbourhood of the instability, which typically occurs near the reattachment point of the laminar reversed flow, are examined for fine meshes and with the semi-coarsening multigrid RNS procedure.

2. GOVERNING EQUATIONS AND BOUNDARY CONDITIONS

The RNS equations for steady, two-dimensional, compressible flow, written in conservation form and in a sheared Cartesian co-ordinate system (ξ, η), are given as follows:

continuity

$$(\rho u)_\xi + (\rho v)_\eta = 0; \tag{1}$$

x-momentum

$$(\rho u^2)_\xi + y'_b(\rho uv + y'_b\rho u^2)_\xi + [(1+y'^2_b)\rho uv + y'_b\rho v^2]_\eta + p_\xi - \frac{1}{Re}(\mu u_\eta)_\eta = 0; \tag{2}$$

y-momentum

$$(\rho uv + y'_b\rho u^2)_\xi + (\rho v^2 + y'_b\rho uv)_\eta + p_\eta = 0; \tag{3}$$

constant stagnation enthalpy

$$T+\frac{\gamma-1}{2}M_\infty^2[u^2+(v+y_b'u)^2]=\text{constant}=H_\infty; \tag{4}$$

equation of state and laminar viscosity relationship

$$p=\frac{\rho T}{\gamma M_\infty^2}, \qquad \mu=T^w. \tag{5}$$

Equations (1)–(5) are given in dimensionless, primitive variable form. M_∞ is the free-stream Mach number and Re is the Reynolds number based on free-stream conditions and some reference length. The shearing transformation is particularly useful for the smooth bump and trough geometries and also simplifies the application of the boundary conditions. The transformation from Cartesian (x, y) to sheared coordinates (ξ, η) is given by

$$\xi=x, \qquad \eta=y-y_b(x). \tag{6}$$

The Cartesian normal or y-component of velocity V is related to the transformed velocity v by

$$v=V-y_b'u. \tag{7}$$

In (6) and (7), $y_b(x)$ defines the body surface and y_b the slope of the surface.

Inflow boundary conditions are specified on u, v, ρ and p, and an outflow boundary condition is required only for p. In the η-direction, one boundary condition is required for each of v and ρ, and two for u. For the geometries discussed in this paper, at the inflow the conditions $u=1$, $v=0$, $\rho=1$ and $p=p_\infty=1/\gamma(M_\infty)^2$ are prescribed for all y, except that $u(y=0)=0$. For the trough geometry, u and v at the inflow $x=1$ are prescribed from a boundary-layer-type marching computation with the RNS equations from $x=0$ to $x=1$, with the axial pressure gradient term explicitly set to zero. For all the present cases, the outflow condition on pressure was $p_x=0$. In the η-direction, the boundary conditions applicable for the geometries considered herein are $u=0$ and $v=0$ at $\eta=0$, and $u=1$ and $\rho=1$ at $\eta=\eta_{max}$. The RNS approximation, equations and boundary conditions are discussed more completely in several papers; see e.g. References 1–3.

3. NUMERICAL DISCRETIZATION AND RELAXATION SCHEME

The mechanism in the RNS equations that provides acoustic or upstream influence is the coupling between the streamwise pressure gradient term in the 'axial' momentum equation and the axial convection term in the 'normal' momentum equation. Axial flow diffusion as well as all diffusion terms in the normal momentum equation (3) are assumed to be negligible; therefore the equations contain only convective and pressure axial flow derivatives. These are first order with respect to the streamwise coordinate ξ so that solutions can, in principle, be obtained by marching in the streamwise direction with prescribed initial conditions. However, for well-posedness of the initial value problem, it is known that only a portion (ωp_ξ) of the pressure gradient term can be retained. The factor ω is given by

$$\omega=\min\{f(M_\xi), 1\}, \qquad f(M_\xi)=\gamma M_\xi^2/[1+(\gamma-1)M_\xi^2], \tag{8}$$

where M_ξ is the Mach number of the streamwise velocity component u.

In order to retain the full elliptic behaviour, the pressure gradient differencing must reflect the boundary value character associated with subsonic flow regions. Rubin[5] has shown that the required pressure gradient discretization can be arrived at with a new form of flux vector splitting

that depends somewhat on the assumed form of the energy equation. For constant stagnation enthalpy, ω is given by (8) and the pressure gradient splitting is given by

$$\omega(p_\xi)_h + (1-\omega)(p_\xi)_e,$$

where $(p_\xi)_h$ is the 'hyperbolic' portion of the pressure gradient, which is backward differenced and reflects a positive flux eigenvalue, and $(p_\xi)_e$ is the 'elliptic' portion of the pressure gradient, which is forward differenced and reflects a negative flux eigenvalue to allow for upstream propagated waves or influence. In particular, for incompressible flow p_ξ is completely forward differenced. This was first shown numerically by Rubin and Lin[6] with a linear stability analysis. The interpretation of this differencing has been discussed with reference to a staggered grid in earlier studies.[1] Rubin has also shown that cell averaging of ω will improve the accuracy of the pressure gradient discretization.[5] For the convective terms, ξ-derivatives are upwind differenced to first- or second-order accuracy. This follows directly from the eigenvalue analysis[5] and reflects the characteristic domain of dependence. For attached flows, this implies backward differencing of these terms. For reversed flow regions, $\omega = 0$ and these convective terms are omitted (FLARE approximation) or are forward differenced.

The continuity equation is discretized about $(i, j\text{-}1/2)$, the x-momentum equation about (i, j) and the y-momentum equation about $(i, j+1/2)$. All η-derivatives are represented with second-order accurate two- or three-point central differences.

The discretized system leads to a set of coupled non-linear equations for u, v, ρ and p. The solution operator S^h applied here is of the iterative line relaxation type. The equations are written at a given streamwise station (ξ = constant line, indexed by i) and are solved to a prescribed level of accuracy before proceeding to the next downstream station. The quantities having the index (i) represent the unknowns at the station i. The pressure p_i is eliminated from the momentum equations, in favour of the density and the velocities, with the aid of the constant stagnation enthalpy condition (4) and the equation of state (5). The non-linear terms are quasi-linearized to second order about the previous local iterate (values initially taken from the $i-1$ station or the previous global iteration). The resulting linear system is inverted by a standard LU decomposition. The computed unknowns are used to update the previous iterate and the inversion can be repeated until local convergence is achieved. At any station i, the downstream pressure p_{i+1} appearing in the equations is unknown. This leads to a global iteration process. The equations are marched downstream, with p_{i+1} prescribed from the previous global iteration. The pressure is then updated by the computation at $i+1$. This process is repeated until convergence is achieved; i.e. the change in the pressure field from iteration to iteration is reduced to a prescribed tolerance. For unseparated flows (and for separated flows when the FLARE approximation is used for the ξ-direction convective term in the ξ-momentum equation), the algorithm requires storage of only the pressure field; the velocities are generated during each marching sweep. If upwind or flux vector splitting[5] differencing is used for separated flows, the velocities are stored in the separation region only. It should be noted here that numerical information from the flow at any downstream location propagates upstream only one mesh width per global iteration. This is typical of line relaxation smoothers.

The stability and convergence properties of the global relaxation procedure have been investigated in previous studies. This analysis shows that the asymptotic convergence factor or spectral radius of the global iteration procedure is $1 - O[(\Delta\xi/\eta_M)^2]$, where η_M is the normal extent of the subsonic flow region. This shows that for very fine meshes in the ξ-direction and/or large η_M (both of which are frequently necessary to resolve flows with strong interaction), the convergence process, though stable, slows significantly.

The present authors have applied the multigrid technique to significantly accelerate convergence of the global pressure relaxation procedure.[3] The multigrid technique rapidly decreases

the error on a given grid by solving related problems on coarser grids, on which it is relatively inexpensive in terms of computational work. It was shown in Reference 3 that in order to successfully implement the multigrid method for highly stretched grids normal to the body surface, a semi-coarsening algorithm that uses the multigrid idea in only the streamwise direction is necessary.

During the line relaxation procedure, the coupled quasi-linearized equations at each marching station are solved for all flow variables. This local inversion can be repeated to obtain local convergence of the non-linear discrete equations; however, this process is computationally expensive. Moreover, it has been found that local iteration does not significantly improve global convergence. Local non-linear convergence can be specified during the final global iterations in order to satisfy the exact non-linear discretized equations. In most cases, however, converged solutions of the quasi-linearized discrete system are sufficiently accurate and far less expensive.

4. INITIALIZATION IMPROVEMENT

The cases considered in this section are: (i) the flow over a sine-wave bump of height 0·025 at $Re = 100\,000$ and (ii) the flow over a trough of depth $d = 0{\cdot}03$ at a Reynolds number of 80 000. The solution to the flow over a sine-wave aerofoil at zero incidence using the RNS equations was obtained by Ramakrishnan and Rubin.[4] The solution to the second problem using the RNS model was first obtained by Reddy.[1] In an earlier paper, Himansu and Rubin[3] used this case as a model problem to demonstrate the efficiency of the semi-coarsening multigrid acceleration technique. For those computations, the initial approximation for the pressure field was always a uniform distribution corresponding to the free-stream value.

In the present work, the effect of initial approximation on the convergence behaviour is examined. The motivation for this study arises from the extreme sensitivity of the convergence to the initial guessed pressure value, as found in earlier calculations for high-Re separated flows. For the computations at higher Re values and for more severe body geometry and finer grids, the calculations even fail to complete a single relaxation pass when free-stream conditions are initially assumed. This is a common difficulty with relaxation methods or iterative fluid dynamic computations. The usual method of circumvention is to first compute the flow for a lower Re and/or less severe body geometry (with free-stream conditions as the initial guess). This converged solution becomes the initial approximation for a more severe problem. The drawback of such a continuation procedure is the additional computational time required or the storage of a 'starting solution' for a given class of flows. This is particularly inefficient if several intermediate-Re/geometry solutions are required. This drawback is extremely limiting when the flow computation is part of an aerodynamic design process.

In this study, three simple techniques to economically extend the Re and body geometry range for computations started with uniform flow initialization are examined. For one application, we examine the flow over a sine-wave bump of maximum height 0·025 at $Re = 100\,000$. The Reynolds number is based on free-stream velocity and unit length. The Reynolds number based on the bump height is 2500. The geometry consists of a flat plate $y_b = 0$ from $x = 0{\cdot}5$ to $x = 0$ followed by a sine-wave profile

$$y_b = 0{\cdot}25[1 + \sin(2\pi x - \pi/2)]$$

from $x = 0$ to $x = 1$, and finally another flat plate segment from $x = 1$ to $x = 2{\cdot}5$. A uniform step size in the ξ-direction of 0·0125 was prescribed. The minimum grid spacing normal to the wall was 0·001 with 121 points and a linear stretching factor of 1·07. As described in Section 3, local iterations are to be avoided except during the last few global iterations. For the test case, when the pressure is initialized with the free-stream value and no local iterations are performed, the

calculations fail at a station just beyond the separation point during the first global pass. Figures 1 and 2 display the computed skin friction parameter and pressure coefficient respectively up to the point of divergence. Attention is now focused on three techniques that overcome this difficulty.

The first strategy is the familiar one of underrelaxation. The particular form used here is the introduction of 'temporal terms' into the governing equations. The temporal terms have the form of the time derivatives in the conservation equations for unsteady flow, so that the governing equations now appear as the 'time-consistent' RNS equations. This is a naturally stable method of allowing the effect of the initialization to damp out. These 'time derivatives' are removed when the solution has evolved sufficiently. The time derivatives are approximated by a backward difference, and the value of the 'temporal step size' Δt is used to control the degree of underrelaxation. The value of the underrelaxation parameter Δt may vary with space as well as with global iteration

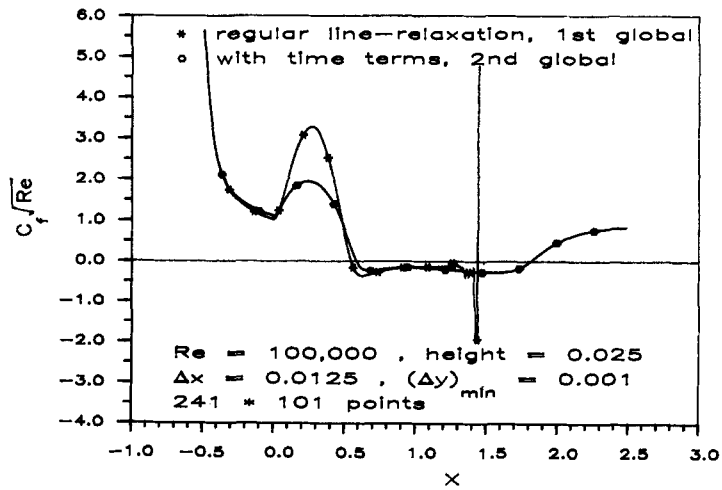

Figure 1. Sine-wave bump: skin friction

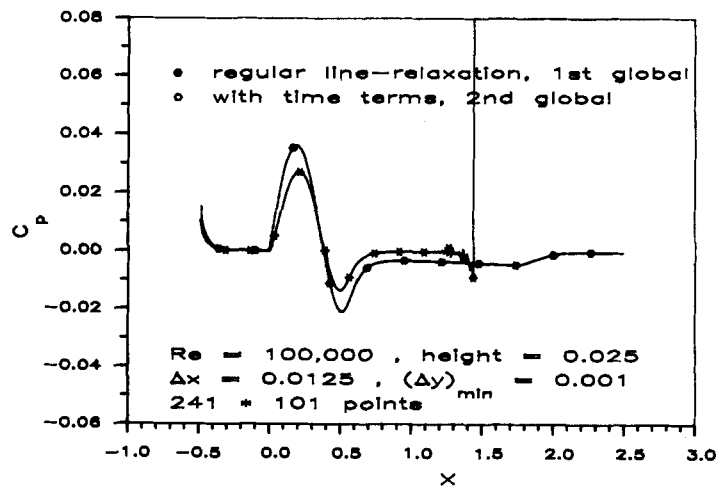

Figure 2. Sine-wave bump: pressure coefficient

number. Large value of Δt correspond to little or no underrelaxation, while $\Delta t = 0$ results in total underrelaxation, i.e. the local solution does not evolve at all. The important difference in this strategy as compared to the use of a time-dependent scheme is that the quasi-linearized velocities required at the 'previous time level', at any station, are not obtained from the previous global iteration but from the previous station. Thus the temporal terms act to lessen the change in velocities and density from one station to the next. Further, these terms are introduced only in regions of flow separation and therefore do not require global storage of the velocities.

The solution computed during the second global iteration with $\Delta t = 10$ is also shown in Figures 1 and 2. The solution is now stable, and although the separation region extends to the downstream boundary during the first global pass, it is much reduced during the second; see Figure 1. During succeeding global passes, the separation region further diminishes and the time term can be phased out. Use of the large value $\Delta t = 10$ is possible since the assumed velocity values at both the previous and current time levels, at each station (i), are taken to be the computed values at the previous station ($i-1$). This is equivalent to quasi-linearizing about the previous station when local iteration is not performed. In this way, the strong convective influence of the attached flow is rapidly propagated downstream. This is in contrast to consistent time-dependent procedures, for which many small time steps are generally required in order to relax from such severe initial conditions. These procedures also require full global storage of the velocities.

The second technique consists of approximately computing the inviscid flow past the same geometry, and using this solution to initialize the pressure field for the RNS computations. For large-Re flows with moderate separation, the pressure field is close to the inviscid pressure field and, as we recall, the primitive variable RNS formulation only requires an initial guess for the pressure field. Full Navier–Stokes iterative solvers would require initial approximations for the velocities as well. The inviscid approximation can be computed by using the RNS code with $u = 1$ as the inflow condition and by replacing the no-slip condition at $\eta = 0$ with the ξ-momentum equation and appropriate reflection conditions to simulate the injection velocity values. The Reynolds number can be maintained at a finite large value since the viscous terms will be negligible; however, Re can also be set to an arbitrary large value if required. A few inviscid global iterations are usually sufficient to establish a reasonable pressure field, since it is the viscous–inviscid interaction that typically slows convergence. Alternatively, any fast efficient inviscid flow solver may be used to obtain the pressure field. It may be noted that a completely converged inviscid solution may not be as effective as a partially converged one. This is due to the fact that the displacement effect of the viscous flow smooths out large surface curvature regions of the body. These geometric effects will be a feature of the converged pressure field of the inviscid portion of the flow.

Figures 3 and 4 display the solution computed during the first viscous flow global sweep, after nine inviscid global iterations. It is seen that the separation region is very small and does not lead to the problems seen with the uniform pressure field. During succeeding global iterations, the separation region gradually enlarges to its converged value.

The third technique discussed here takes advantage of the fact that often computations that break down due to poor initialization can be successfully carried out with exactly the same initialization but on sufficiently coarse grids. An approximate solution is obtained to the problem on such a coarse grid and is interpolated as an initialization onto the grid on which the solution is desired. If the first grid is relatively too coarse to make interpolation useful, a hierarchy of grids may be used, with a quick approximate solution on each grid being interpolated as the initialization for the immediately finer grid. Such a process forms a natural part of the Full MultiGrid algorithm. However, this was not used in Reference 3, where calculations were always started on the finest grid. Figures 3 and 4 also show the solution computed during the first global

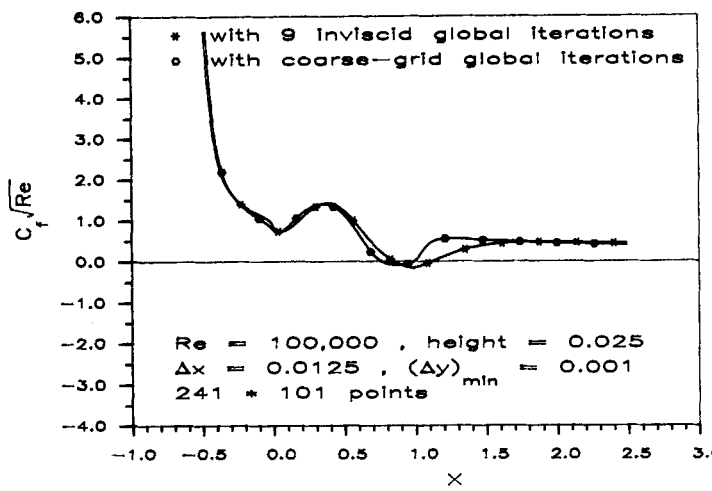

Figure 3. Sine-wave bump: skin friction

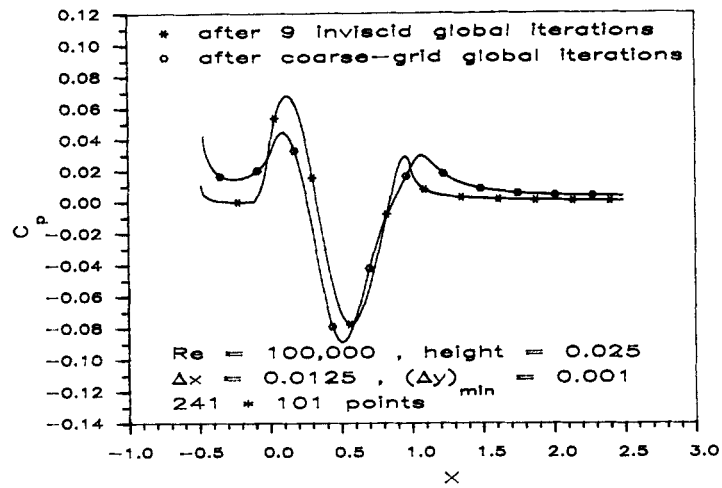

Figure 4. Sine-wave bump: pressure coefficient

iteration on the fine grid after initialization with the pressure computed on a coarser grid. The coarse grid was formed by selecting alternate $\xi =$ constant lines of the fine grid, and the computed pressure was linearly interpolated in the ξ-direction onto the fine grid. It is seen that the calculations have proceeded smoothly through the separation region. Converged solutions for this flow are not displayed here, as they are not of primary interest in the discussion.

The techniques for improvement of the initial guess have merit not only in severe cases where the line relaxation would otherwise break down, but also in more moderate cases where the relaxation would not fail but would require many global iterations to converge to within a prescribed tolerance. The advantage of these techniques for the latter flows is the computational work saved in achieving the converged solution. To illustrate this we consider the flow over a trough of depth 0·03 at $Re = 80\,000$ based on unit length. The Reynolds number based on trough

depth is 2400. The trough is assumed to begin at $x=0$. The computation is carried out from $x=1$ to $x=4$. A boundary layer computation from $x=0$ to $x=1$ provides the inflow conditions at $x=1$. The grid used is the same as in the sine-wave bump case. The trough geometry, centred at $x=2{\cdot}5$, is given by

$$y_b = -d\,\mathrm{sech}\,[4(x-2{\cdot}5)],$$

where d is the depth of the trough. The first pressure iterates with and without preliminary inviscid global iterations are compared in Figure 5. Also shown is the converged solution, as a basis for judging how close the iterates are to the desired solution. It is seen that use of a few (six) preliminary inviscid iterations significantly moves the pressure field towards the final solution. This may also be seen from the residual norm in the two cases, which is shown plotted against computational work (in units of global iterations) in Figure 6.

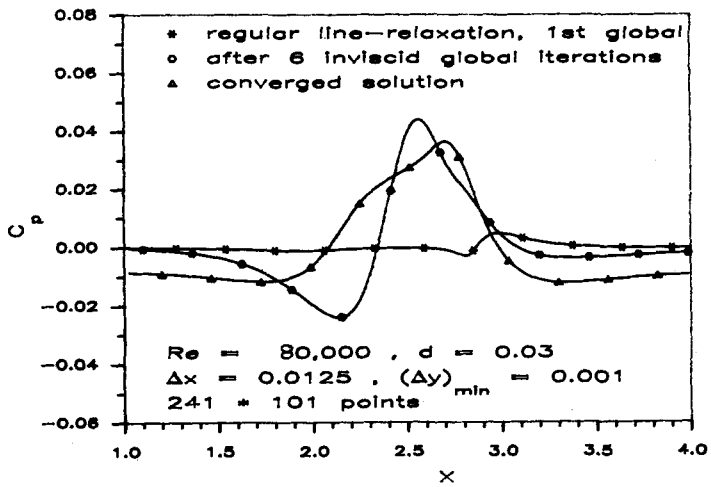

Figure 5. Trough: pressure coefficient

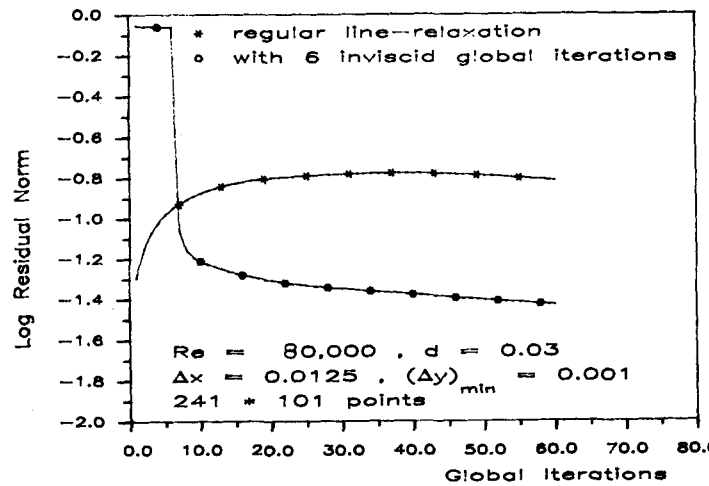

Figure 6. Trough: convergence history

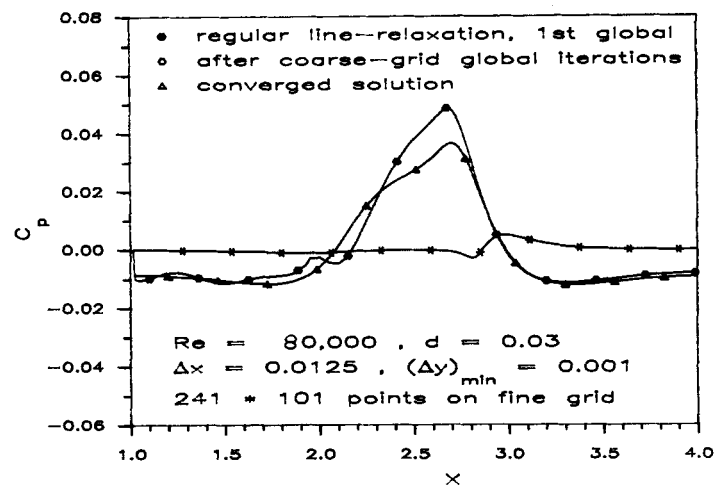

Figure 7. Trough: pressure coefficient

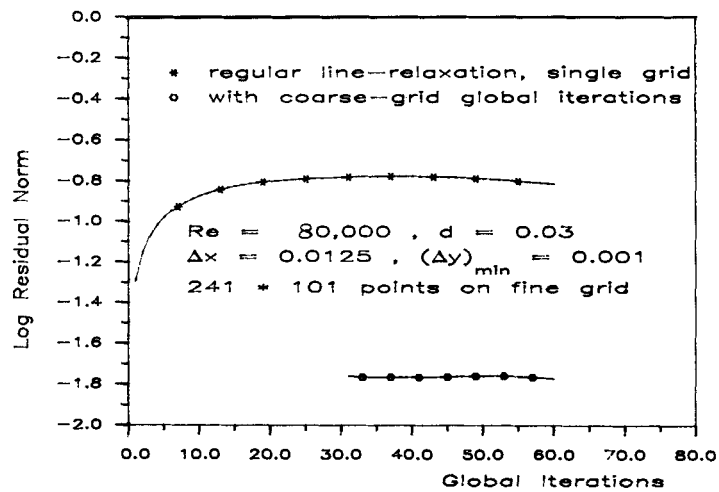

Figure 8. Trough: convergence history

Figure 7 and 8 display a similar gain produced by use of coarse-grid computations interpolated to the fine grid.

5. LAMINAR SEPARATION 'BREAKDOWN'

Multigrid-accelerated calculations were reported in Reference 3 for a trough with $d=0{\cdot}03$ at $Re=80\,000$. A more severe case was then considered for the present study. A solution was attempted for $d=0{\cdot}06$ and $Re=100\,000$. A converged solution was not obtainable for this problem when a sufficiently fine grid was prescribed. It is believed that the reason for this failure lies not in the multigrid algorithm or the line relaxation process but in the physics of the flow.

Figure 9 depicts the skin friction parameter for converged solutions with axial step sizes $\Delta\xi=3/144$ and $\Delta\xi=3/192$. Upwind differencing of the streamwise convective term in the

streamwise momentum equation was used in both these cases. Nearly identical solutions are obtained when the FLARE approximation is used for this term. The streamwise extent of the separation region is much greater than in the case of the $d = 0{\cdot}03$ trough. Noteworthy is the 'dip' in the curves prior to reattachment and the steepening of the dip with decreasing mesh size. Figure 10 shows the coefficient of pressure c_p versus axial distance for the same cases. A converged solution for a slightly finer streamwise mesh of size $\Delta\xi = 3/200$ is shown in Figures 11 and 12. Both skin friction and pressure display oscillations within the flow reversal region, near reattachment. Further refinement of the streamwise grid results in a total breakdown of the computation. No converged solution was obtainable. The streamwise step size should be small enough to resolve most features of the flow; however, the instability could not be resolved with further grid refinement. A physical laminar flow breakdown is suggested. The mesh in the η-direction is

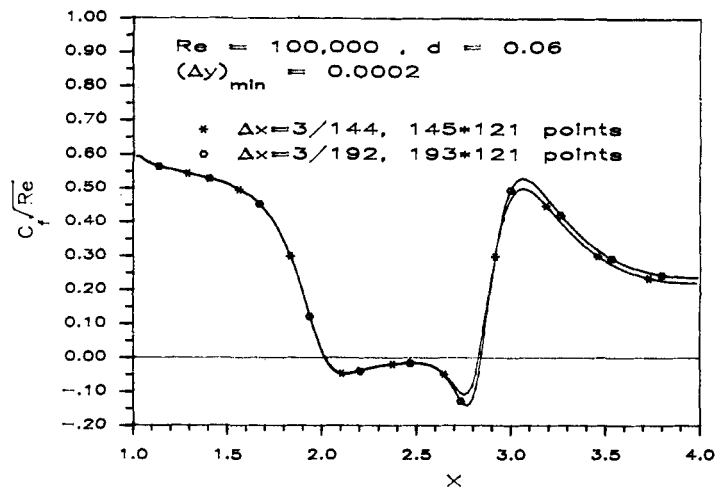

Figure 9. Trough: skin friction parameter

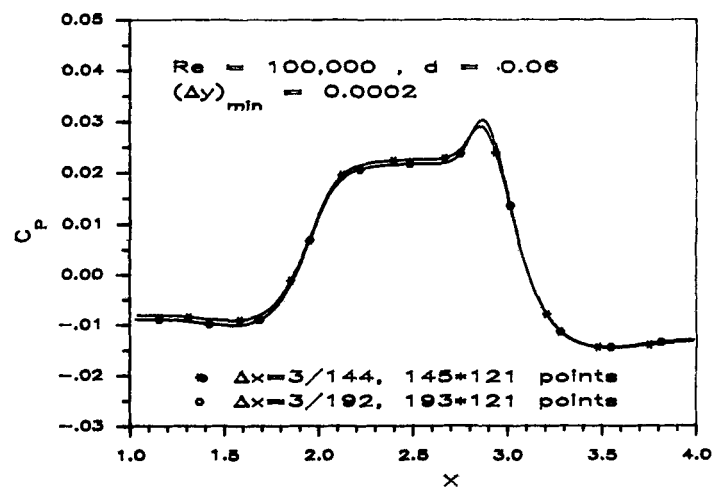

Figure 10. Trough: coefficient of pressure

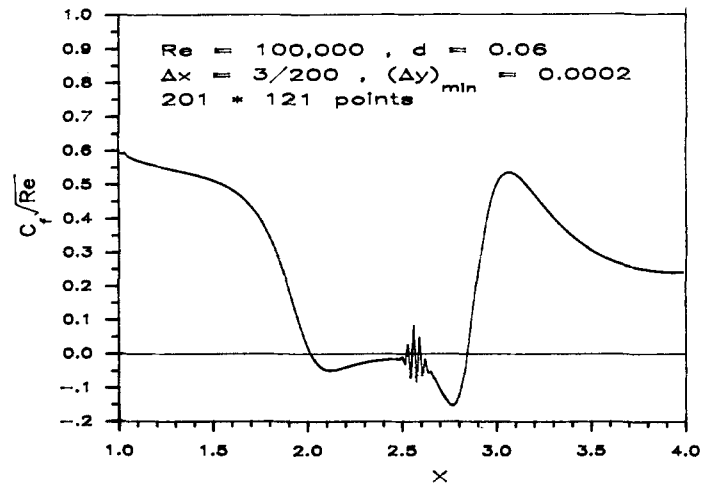

Figure 11. Trough: skin-friction parameter

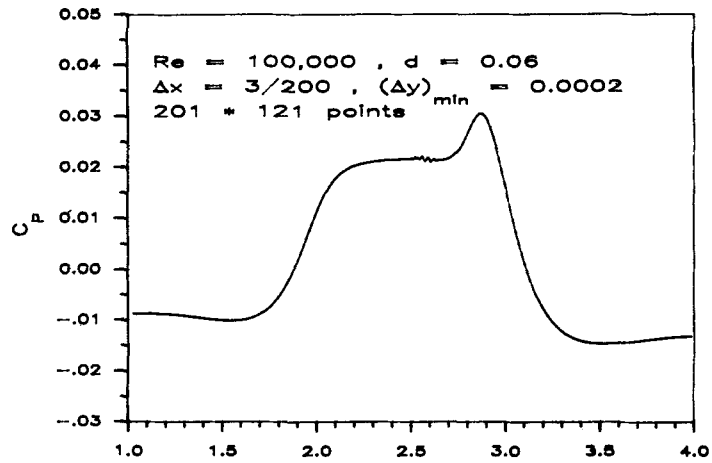

Figure 12. Trough: coefficient of pressure

adequately fine, as shown by the solution in Figure 13, where halving of the wall value of $\Delta\eta$ did not produce any noticeable change in the solution.

The breakdown cannot be attributed to poor initialization of the calculations since converged solutions on coarser grids were used as the initial guesses. Additionally, the calculation on a fine axial grid was started with free-stream conditions, and the solution proceeded normally for a while. The breakdown was observed only after the solution had evolved sufficiently. Ramakrishnan and Rubin[4] have described a similar phenomenon in the flow past a sine-wave aerofoil at zero incidence and sufficiently high *Re*. Their solutions were obtained with the time-consistent form of the RNS equations and display similar abrupt reattachment. In the same manner as in the present study, the dip in skin friction increases as the mesh is refined, and no solution could be obtained for finer meshes. Additional evidence suggesting a physical mechanism for the breakdown comes from the calculations of Bender and Khosla,[7] who used a direct solver

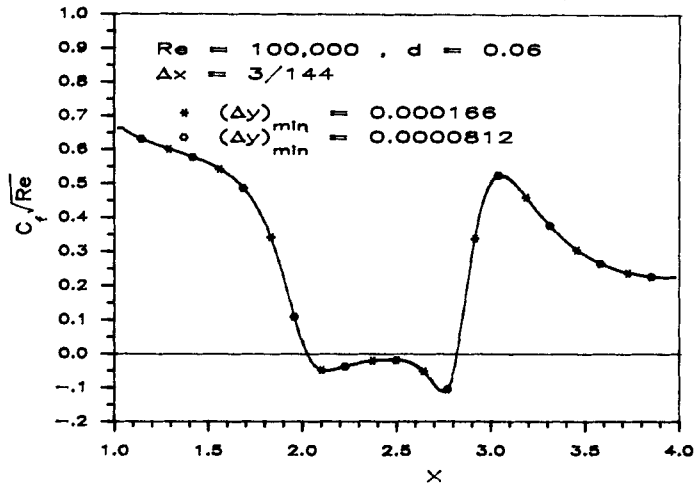

Figure 13. Trough: skin friction on fine y-grids

for the steady-state form of the streamfunction–vorticity system for the flow past the sine-wave aerofoil. They too found that at sufficiently high Re, the dip in surface shear increases significantly as the mesh is refined. Moreover, when temporal terms were added, the solution became unbounded for all but very large values of Δt.

Experimental results have not been obtained for the trough configuration; the flow separation for this case may be expected to have the same qualitative features as the marginal separation encountered behind the rounded leading edge of aerofoils at small or zero incidence and sufficiently high Re. The latter case is known to often involve a transitional separation bubble with abrupt turbulent reattachment and has been extensively studied during the past few years. It has been shown by several authors (see e.g. Smith and Elliott[8]) that the transition to turbulence is controlled by local features of the flow. In a recent paper, Davis *et al.*[9] have found excellent agreement with experiment for flow over an aerofoil with a small transitional separation bubble. They applied a correlation proposed by Roberts to specify the transition point in the reversed flow region. According to the correlation as presented in Reference 9, the transition Reynolds number based on surface length from the separation point, for negligible free-stream turbulence level, is about $0{\cdot}58 \times 10^5$. If the correlation were applicable in the case of the present trough calculations, this would put transition within the separation bubble at approximately $x = 2{\cdot}6$.

One theoretical approach to the stability of marginal separation may be found in a paper by Smith and Elliott.[8] That study and that of Davis *et al.*[9] were prompted in part by renewed interest in laminar flow control and general drag reduction techniques. Order-of-magnitude and perturbation analysis of the boundary layer indicates that a non-linear accumulation resulting in a 'shock-like' reattachment structure can occur in separated flows. The upstream part of the structure has a strong reversed motion with an abrupt but smooth adjustment to strong forward motion. The resemblance between this structure and the 'shock' terminating the flow reversal in the trough computations is deemed significant by the present authors. Smith and Elliott go on to link their non-linear breakdown to possible transition to turbulence and to the abrupt turbulent reattachment of marginal laminar separation that is often observed near aerofoil leading edges. These studies suggest that the nature of breakdown found in the present trough calculations with mesh refinement may represent a physical instability in the flow and may be indicative of incipient

transition to turbulence. Full three-dimensional claculations would be required to model this behaviour.

In view of this possibility, a turbulence model was introduced into the calculations. The model employed was the two-layer model of Baldwin and Lomax.[10] The turbulence appears in the governing equations through the coefficient of viscosity in equation (5) such that $\mu = T^w + Re\,\mu_t$, where μ_t is the eddy viscosity. The eddy viscosity model is assumed to obey Prandtl's mixing-length hypothesis in the inner layer, and it takes a form similar to the Clauser formulation in the outer layer. The advantage of the model over other algebraic eddy viscosity models is that it does not require evaluation of the displacement thickness of the boundary layer. More details of the model may be found in Reference 10. The eddy viscosity is uncoupled from the local inversion and is updated during local iterations to convergence. A streamwise intermittency factor was used to simulate the transition process. Transition was initiated at $\xi = 2{\cdot}15$, i.e. just beyond the separation point. It is seen from Figure 14 that the turbulence greatly changes the nature of the solution. The dip in the skin friction is no longer present and the reattachment occurs within a much shorter distance. Moreover, this solution does not exhibit any 'instability' even for very fine grid solutions as obtained with the semi-coarsening multigrid procedure. The solution is computable on all grids considered herein; axial grid refinement from $\Delta\xi = 3/288$ to $\Delta\xi = 3/576$ does not alter the solution appreciably. The slight kink in the skin friction curve at its lowest point is due to the turbulence model. The computed eddy viscosity displays a small discontinuity at that location. This is perhaps due to the appearance of double peaks in the vorticity function.

Attention was next turned to the effect of boundary layer control with surface suction. Wall suction was simulated by replacing the $v = 0$ condition at $\eta = 0$ by $v = v_s$, where v_s is an injection velocity in the η-direction. Although the 'suction' thus specified is in the η-direction and not normal to the surface, it will display the same qualitative features as normal suction. Figure 15 displays the skin friction parameter versus axial distance for suction velocities of 0·002 and 0·003. It is seen that 0·002 is insufficient suction to remove the 'dip' in the curve, while 0·003 removes the flow separation altogether. As seen in Figures 16 and 17, a suction velocity of 0·0025 markedly changes the character of the separated flow without eliminating flow reversal. The pressure plot in particular shows that the separation region has a smoothly varying wall pressure at reattachment. This solution is obtained on a finer grid than was possible without the suction. With the multigrid

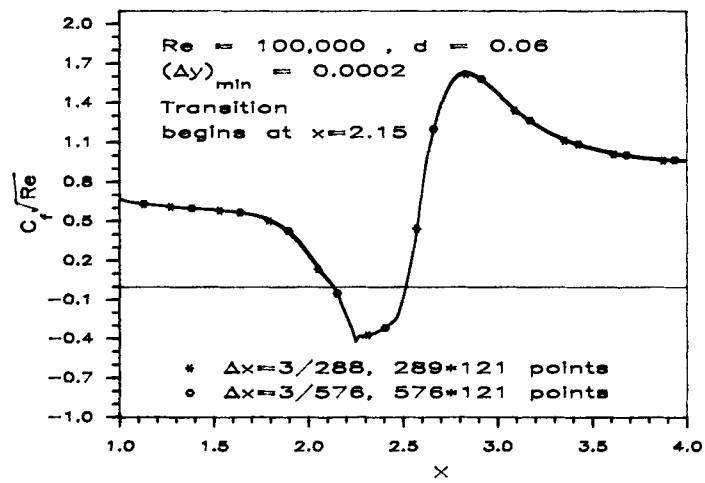

Figure 14. Trough: effect of turbulence

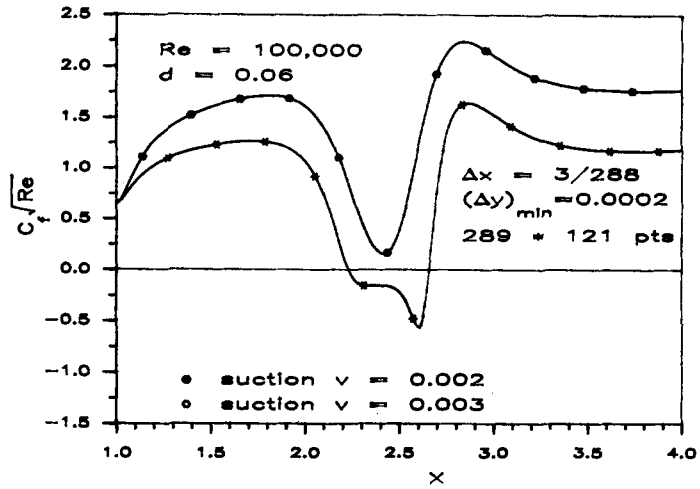

Figure 15. Trough: effect of wall suction

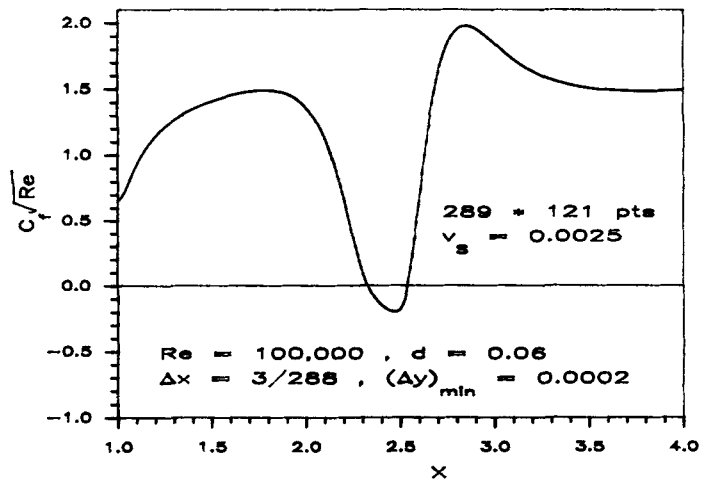

Figure 16. Trough: effect of wall suction

procedure the grid can be further refined to obtain solutions in an efficient and economic manner. These results do not exhibit any essential change in the quantitative nature of the solution. This result, together with those for the turbulence model presented in the previous paragraph, reinforce the hypothesis that the breakdown found for the laminar computations is a physical rather than numerical instability, and occurs when the Reynolds number based on the depth of the trough is sufficiently large. Significantly, these results draw attention to the critical need for fine-mesh calculations and grid refinement studies in all computations of high-*Re* laminar separated flows.

6. CONCLUSIONS

The convergence properties of RNS global relaxation were examined with a very efficient semi-coarsening multigrid accelerator. Very fine axial meshes and highly stretched very fine surface-normal meshes were considered. Three techniques were proposed to enhance convergence of the

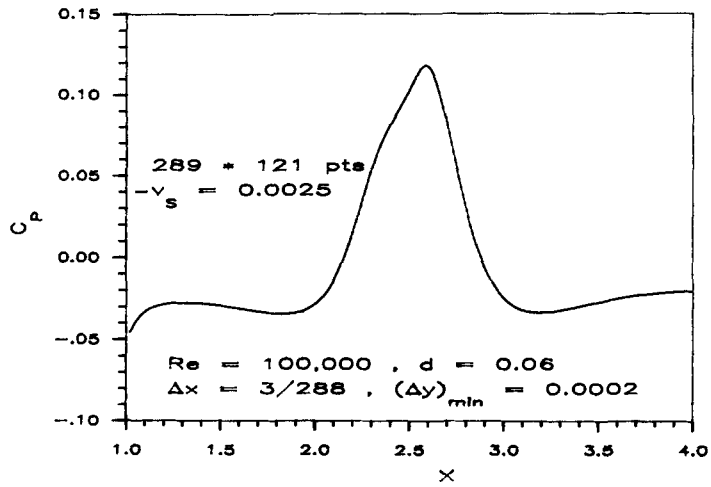

Figure 17. Trough: effect of wall suction

RNS relaxation procedure, even for rather arbitrary starting conditions and without expensive initialization procedures. The use of temporal terms for underrelaxation, the use of preliminary inviscid flow iterations and of coarse-grid iteration to initialize the pressure field were each successful in eliminating divergence due to severe initial conditions for the flow past a sine-wave bump. The last two techniques also economically reduce the initial error for convergent computations and thereby greatly enhance the efficiency of convergence.

The laminar flow over a deep trough of depth 0·06 and $Re = 100\,000$ was a severe test case. It was found that on a sufficiently fine streamwise grid a local breakdown occurred. Careful grid refinement studies could not remove this instability. Comparison of the calculated flow behaviour with Navier–Stokes and time-consistent RNS solutions, with experimental and other computational results for aerofoil leading-edge separation and with asymptotic analysis of marginal laminar separation leads to the belief that the breakdown is indicative of a physical instability. This instability occurs in even marginally separated flows and results in a shock-like reattachment. The instability is possibly indicative of incipient transition to turbulence. The introduction of a turbulence model beyond the separation point was found to suppress the instability. The application of small wall suction also removed the instability, even when the flow reversal was still present. These results underline the need for sufficient grid refinement in all high-Re laminar separated flow calculations. Full three-dimensional calculations would be required to capture the transition phenomenon, if in fact this is the driving mechanism resulting in the two-dimensional breakdown.

REFERENCES

1. S. G. Rubin, 'Incompressible Navier–Stokes and PNS formulations and computational techniques', in W. G. Habashi (ed.), *Computational Methods in Viscous Flows, Vol. III*, Pineridge Press, Swansea, 1984.
2. S. G. Rubin and D. R. Reddy, 'Analysis of global pressure relaxation for flows with strong interaction and separation', *Comput. Fluids*, **11**, 281–306 (1983).
3. A. Himansu and S. G. Rubin, 'Multigrid acceleration of a relaxation procedure for the RNS equations', *AIAA J.*, **26**, 1044–1051 (1988).
4. S. V. Ramakrishnan and S. G. Rubin, 'Time-consistent pressure relaxation procedure for compressible reduced Navier–Stokes equations', *AIAA J.*, **25**, 905–913 (1987).

5. S. G. Rubin, 'RNS/Euler relaxation as a form of flux-vector splitting', *Comput. Fluids*, **16,** 485–490 (1988).
6. S. G. Rubin and A. Lin, 'Marching with the PNS equations', *Israel J. Technol.*, **18,** (1981).
7. E. E. Bender and P. K. Khosla, 'Application of sparse matrix solvers and Newton's method to fluid flow problems', *Proc. Natl Fluid Dynamics Congr.*, Cincinnati, July 1988, Paper 88–3701.
8. F. T. Smith and J. W. Elliott, 'On the abrupt turbulent reattachment downstream of leading-edge laminar separation', *Proc. R. Soc. Lond. A*, **401,** 1–27 (1985).
9. R. L. Davis, J. E. Carter and E. Reshotko, 'Analysis of transitional separation bubbles on infinite swept wings', *AIAA J.*, **25,** 421–428 (1987).
10. B. S. Baldwin and H. Lomax, 'Thin layer approximation and algebraic model for separated turbulent flows', *AIAA Paper 78–257*, 1978.